ELSEVIER

Materials Science and Engineering A 490 (2008) 335–342

MATERIALS SCIENCE & ENGINEERING A

www.elsevier.com/locate/msea

Evolution of microstructure and texture in an ultrafine-grained Al6082 alloy during severe plastic deformation

Sandip Ghosh Chowdhury [a,*], Amit Mondal [a], Jenő Gubicza [b], György Krállics [c], Árpád Fodor [c]

[a] *Materials Science & Technology Division, National Metallurgical Laboratory, Jamshedpur 831007, India*
[b] *Department of Materials Physics, Eötvös University, P.O. Box 32, H-1518 Budapest, Hungary*
[c] *Department of Materials Science and Engineering, Budapest University of Technology and Economics, H-1521 Budapest, Hungary*

Received 13 December 2007; received in revised form 11 January 2008; accepted 16 January 2008

Abstract

The evolution of microstructure and texture in Al6082 precipitation-hardened alloy during equal-channel angular pressing (ECAP) was studied. It was found that although the dislocation density and the subgrain size saturated after 1 pass, the size of grains bounded by high angle boundaries reached its minimum value only after 4 passes. Furthermore, the grain orientation distribution changes between 4 and 8 passes, indicating the development of grain boundary structure even after the saturation of the parameters of the microstructure. As a result of this evolution, the initial texture of the commercial alloy was diminished after 8 passes and the grain orientation distribution became to be close to random case.

Keywords: Equal-channel angular pressing; Aluminium alloy 6082; Crystallographic texture; Dislocation density; Grain boundary misorientation distribution

1. Introduction

Equal-channel angular pressing (ECAP) is an effective method for reducing the grain size to, typically, the submicrometer level by introducing large plastic strain into materials through repetitive processing. The ultrafine-grained (UFG) materials produced by ECAP have a very high strength due to their low grain size and high dislocation density [1]. As severe plastic deformation (SPD) procedures enable to produce UFG materials in bulk shape, there is an increasing interest for these materials with respect to their technological applications. This interest is especially large for SPD processing of those materials which are traditionally basic materials in the industry (e.g. precipitation-hardened Al alloys).

For understanding the mechanical behavior of UFG materials produced by ECAP, it is necessary to characterize their microstructure. A comprehensive review on the development of UFG materials via ECAP has been published recently [2]. In the early stage of grain refinement during ECAP, dislocation cell structures with low angle grain boundaries (LAGBs) develop. LAGBs are usually in non-equilibrium state [3,4], hence it is expected that they would transform into a more equilibrated high angle grain boundaries (HAGBs) in further deformation [5,6].

During the formation of HAGBs, there are substantial grain rotations; therefore, it is expected that texture develops in materials subjected to ECAP processing. Detailed investigations have been conducted to evaluate the texture evolution in various Al alloys processed by ECAP [7–13]. The results from these experiments show similarities between the textures formed during ECAP and those introduced by large strain in a simple shear, however, there are also additional rotations occurring when the sample passes repetitively through the ECAP die [14]. Depending on the nature of precipitates, the texture evolution is different in precipitation-hardened Al alloys. Experiments carried out on Al5056 and Al2024 alloys showed gradual increase in texture strength with increasing number of passes [7,15]. At the same time, for Al7034 alloy it has been observed that there was an initial weakening and a subsequent strengthening of the overall texture as the strain increased [16].

In this paper the evolution of the microstructure and the texture in Al6082 commercial alloy as a function of number of

* Corresponding author. Tel.: +91 657 2271709x2052; fax: +91 657 2270527.
E-mail address: sandipgc@gmail.com (S.G. Chowdhury).

0921-5093/$ – see front matter © 2008 Elsevier B.V. All rights reserved.
doi:10.1016/j.msea.2008.01.049

ECAP passes are studied. The grain boundary misorientation distribution is also determined for different ECAP passes. To the knowledge of the authors such a complex characterization of the grain size, subgrain size, defect structure and texture of the ECAP-processed Al6082 alloy is missing from the literature.

2. Experimental

A commercial Al–Mg–Si alloy (Al6082) was processed by ECAP. The main constituents of the alloy are Al (97%), Mg (0.6–1.2%), Si (0.7–1.3%) and Mn (0.4–1%) in weight percents. Before ECAP deformation the material was annealed at 420 °C for 40 min in order to homogenize the microstructure. This sample was regarded as the initial state of the material. In the initial material beside the Al matrix a small amount of Mg_2Si and $Mn_{12}Si_7Al_5$ phases have been identified by X-ray diffraction [17]. Cylindrical billets of 15 mm in diameter and 145 mm in length were pressed through the ECAP die with $\varphi = 90°$ angle of intersection between the channels. One, four and eight passes were performed by route *C* (the billet was rotated by 180° around its longitudinal axis between intermediate passes) at room temperature and at constant displacement rate of 8 mm/min. The applied load increased from 120 to 180 kN with increasing the number of ECAP passes because of the strain hardening of the alloy. A schematic drawing in Fig. 1 shows the notations of three orthogonal axes of the ECAP-processed billet. The *X*-axis is parallel to the flow direction (ED), the *Y*-axis (ND direction) is perpendicular to the top surface at the point of exit from the die and the *Z*-axis (TD direction) normal to the side face at the point of exit from the die. The three directions can be regarded as the normal vectors of three orthogonal planes of the billet. These planes are denoted by the same letters as the corresponding normal directions.

The microstructure of the initial and ECAP-processed materials was studied by X-ray line profile analysis. The X-ray peak profiles were measured on the cross section (X-plane) of the samples by a high-resolution double-crystal diffractometer (Nonius, FR 591) using Cu $K\alpha_1$ radiation. The peak profiles were evaluated by the multiple whole profile (MWP) fitting procedure

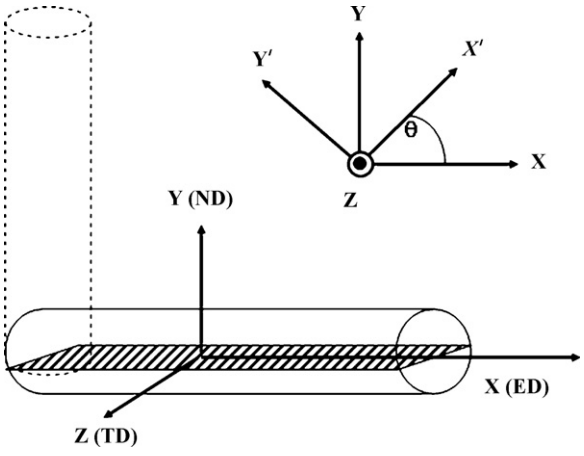

Fig. 1. Schematic picture showing the three orthogonal directions of ECAP-processed billet.

[18,19]. In this method, the Fourier coefficients of the experimental profiles are fitted by the product of the theoretical Fourier transforms of size and strain peak profiles. The theoretical functions used in the fitting are calculated on the basis of a model of the microstructure. In this model, the crystallites have spherical shape and log-normal size distribution, and the lattice strains are assumed to be caused by dislocations. The method gives the crystallite size distribution as well as the density and the arrangement of dislocations. In this study the volume-weighted mean crystallite size ($\langle x \rangle_{vol}$), the dislocation density (ρ) and the dislocation arrangement parameter (M) are presented for the initial and the ECAP-processed specimens. The lower the value of M, the higher the screening of the strain fields of dislocations, i.e. the stronger the dipole character of the dislocation structure [20].

Texture studies were carried out on the initial sample as well as after ECAP. Four incomplete pole figures {1 1 1}, {2 0 0}, {2 2 0} and {3 1 1} were measured up to a reflection angle of 70° by the Schultz reflection method in a Philips X'pert powder diffractometer using a Cu anode. Texture was measured on the Y-plane equivalent to the flow plane at the point of exit from the ECAP die (see Fig. 1). The measurements were carried out in the middle plane section of the billet on an area having dimensions of 15 mm × 10 mm. Before texture measurements the surface was mechanically polished.

The orientation distribution function (ODF) of the grains was calculated from the texture measurements by arbitrarily defined cells (ADC) method after corrections and normalization, without imposing any restriction on the sample symmetry [21]. It has been shown that the samples processed by route *C* have slight through-thickness heterogeneity in both microstructure and the texture [22]. Therefore all measurements have been carried out at the middle plane section of the sample.

The grain boundary misorientation distribution was measured by electron backscatter diffraction (EBSD). These experiments were carried out on the Y-plane of the sample after each ECAP pass by a Quanta 200 FEG-SEM with TSL OIM software.

Tensile tests were carried out using a MTS 810 mechanical testing machine. The velocity of the cross head was kept at 1.8 mm/s. The gauge length of the tensile specimens was 17.5 mm with diameter of 3.5 mm. The longitudinal axis of the tensile specimens was parallel to the longitudinal axis of the ECAP-processed billet (*X*-axis). We could take out six tensile specimens from each workpiece. The yield strength was determined as the average of the 0.2% offset stress values obtained for six samples.

3. Results

3.1. Microstructure from X-ray line profile analysis

The Bragg peaks measured on the cross sections by high-resolution diffractometer were evaluated by MWP fitting procedure. Fig. 2 shows the normalized Fourier coefficients of the measured intensity profiles (open circles) and the fitted theoretical Fourier transforms (solid line) for the specimen deformed by 1 ECAP pass. In the fitting procedure the parameter describ-

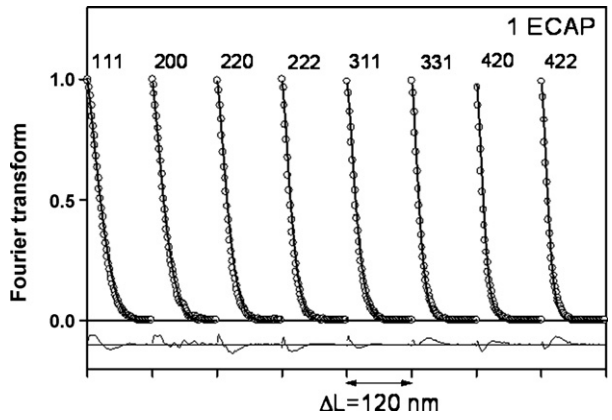

Fig. 2. The measured (open circles) and fitted (solid lines) Fourier coefficients normalized to unity for the sample processed by 1 ECAP pass. The differences between the measured and fitted values are also shown in the lower part of the figure. The scaling of the differences is the same as in the main part of the figure. The indices of the reflections are also indicated.

Table 1
The mean crystallite size ($\langle x\rangle_{vol}$), the dislocation density (ρ) and the dislocation arrangement parameter (M) obtained by X-ray line profile analysis, and the average grain size determined by EBSD (d) and the yield strength for the initial state and for the samples processed by different passes of ECAP

No. of passes	$\langle x\rangle_{vol}$ (nm)	ρ ($\times 10^{14}$ m^{-2})	M	d (μm)	Yield strength (MPa)
Initial state	>500	<0.1	–	20	82 ± 4
1 ECAP	87 ± 9	4.0 ± 0.5	4.4 ± 0.5	4	184 ± 5
4 ECAP	74 ± 9	3.9 ± 0.5	2.2 ± 0.3	1	203 ± 6
8 ECAP	76 ± 9	4.6 ± 0.5	2.2 ± 0.3	1	226 ± 6

ing the edge or screw character of dislocations, i.e. q is fixed to 0.85 assuming half edge–half screw character of dislocations (0.36 for pure edge and 1.33 for pure screw dislocations in Al).

The volume-weighted mean crystallite size ($\langle x\rangle_{vol}$) and the dislocation density (ρ) for the initial state and for the ECAP-processed samples are listed in Table 1. Ultrafine-grained microstructure ($\langle x\rangle_{vol} = 87$ nm) with high dislocation density (4×10^{14} m^{-2}) was achieved even after 1 pass. The crystallite size and the dislocation density change slightly for higher passes. The dimensionless dislocation arrangement parameter, M, has a value of 4.0 ± 0.5 after 1 pass and it decreased to 2.2 ± 0.3 after 4 ECAP passes. This indicates that the dipole character of the dislocation structure and the screening of the displacement field of dislocations became stronger with increasing deformation.

3.2. Texture analysis

For the ECAP textures, the indices $\{h\,k\,l\}\langle u\,v\,w\rangle$ was used to denote an orientation having an $\{h\,k\,l\}$ plane parallel to the Y-plane and a $\langle u\,v\,w\rangle$ direction parallel to the X-direction [2]. To facilitate the description of the texture, Table 2 provides a summary of the Euler angles for the main ideal orientations in shear deformation [23] and for a single ECAP pass for $\varphi = 90^\circ$ (φ is the angle between the intersecting ECAP channels) based on the calculations by Li et al. [24]. In this representation, φ_1 is the rotation angle about Y-axis, ϕ is the angle of rotation about the new X'-axis (X' is obtained from X by rotation about Y-axis with φ_1) and φ_2 is a rotation angle about the final Z'-axis (Z' obtained from Z by the two former rotations about Y and X').

In the coordinate system chosen here, the differences between the observed and the theoretical shear texture components may correspond to shift in φ_1 only, i.e. to a rotation about Y-axis. It has been shown that ECAP orientations can be derived from those of negative simple shear, by increasing the ideal values of φ_1 of a simple shear by θ (=ϕ/2), while the two other Euler angles remain the same [24]. One ECAP pass can be described as a simple shear in the flow plane. Canova et al. [25] have classified f.c.c torsion (shear) textures in terms of three components: A fiber $\{1\,1\,1\}\langle h\,k\,l\rangle$, B fiber $\{h\,k\,l\}\langle 1\,1\,0\rangle$ and C component $\{0\,0\,1\}\langle 1\,1\,0\rangle$, where the notation refers to {plane parallel to the shear plane}<direction parallel to the shear direction>. These orientations, thus derived, are distributed along two partial fibers: $\{1\,1\,1\}_\theta\langle u\,v\,w\rangle$ with a $\{1\,1\,1\}$ plane counter clock wise (CCW) rotated by θ about TD from the ND plane and $\{h\,k\,l\}\langle 1\,1\,0\rangle_\theta$ with a $\langle 1\,1\,0\rangle$ direction CCW-rotated by θ

Table 2
Ideal shear texture components and ideal ECAP texture components

Component	$\{h\,k\,l\}\langle u\,v\,w\rangle$	φ_1	ϕ	φ_2
A	$(1\,\bar{1}\,1)[1\,1\,0]$	0	35.26	45
$\bar{A}$	$(\bar{1}\,1\,1)[\bar{1}\,\bar{1}\,0]$	180	35.26	45
B	$(1\,\bar{1}\,2)[1\,1\,0]$	0/120/240	54.74	45
$\bar{B}$	$(\bar{1}\,1\,\bar{2})[\bar{1}\,\bar{1}\,0]$	60/180	54.74	45
C	$\{0\,0\,1\}\langle 1\,1\,0\rangle$	90/270, 0/180	45, 90	0/90, 45
A_1^*	$(1\,1\,1)[\bar{1}\,\bar{1}\,2]$	35.26/215.26, 125.26	45, 90	0/90, 45
A_2^*	$(1\,1\,1)[1\,1\,\bar{2}]$	144.74, 54.74/234.74	45, 90	0/90, 45
A_θ	$\{1\,1\,1\}_\theta\langle 1\,1\,0\rangle_\theta$	45	35.26	45
$\bar{A}_\theta$	$\{1\,1\,1\}_\theta\langle 1\,1\,0\rangle_\theta$	225	35.26	45
B_θ	$\langle 1\,1\,0\rangle_\theta$	45/165/285	54.74	45
$\bar{B}_\theta$	$\langle 1\,1\,0\rangle_\theta$	105/225/345	54.74	45
$A_{1\theta}^*$	$\{1\,1\,1\}_\theta$	80.26/260.26, 170.26/350.26	45, 90	0, 45
$A_{2\theta}^*$	$\{1\,1\,1\}_\theta$	9.74/189.74, 99.74/279.74	45, 90	0, 45
C_θ	$\langle 1\,1\,0\rangle_\theta$	135/315, 45/225	45, 90	0, 45
{1 1 1} fiber	$\{1\,1\,1\}\langle u\,v\,w\rangle$			
<1 1 0> fiber	$\{h\,k\,l\}\langle 1\,1\,0\rangle$			

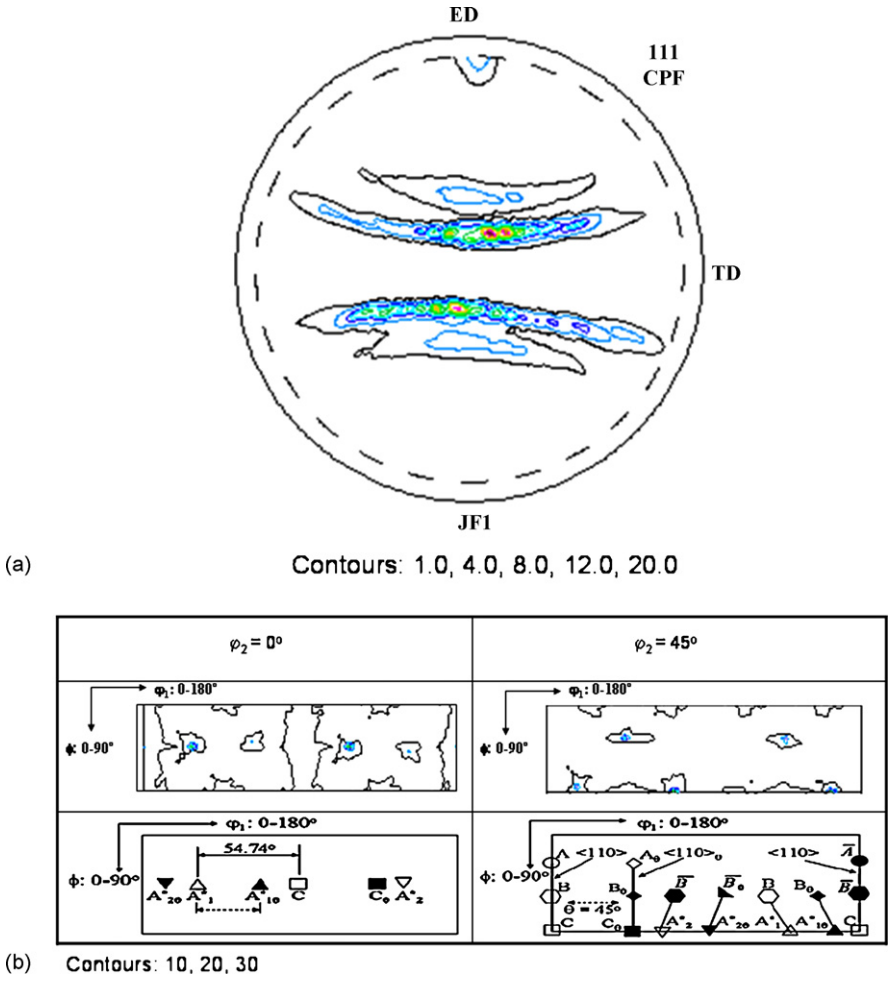

Fig. 3. Texture of the initial material: (a) $\{1\,1\,1\}$ pole figure and (b) ODF sections at $\varphi_2 = 0^\circ$ and 45°.

about TD from ED. The orientation distributions can be represented by three fibers: f1, f2 and f3. The f1 fiber consists of the $A^*_{1\theta}$–A_θ–$A^*_{2\theta}$ $\{1\,1\,1\}_\theta$ partial fiber. The f2 fiber consists of C_θ–$\overline{B}_\theta$–$\overline{A}_\theta$ orientations along $<1\,1\,0>_\theta$ and the $\overline{A}_\theta$–$A^*_{1\theta}$ orientations along $\{1\,1\,1\}_\theta$; the two fibers meet at $\overline{A}_\theta$ position. The f3 fiber which is symmetrical to the f2 fiber described above, contains the C_θ–B_θ–A_θ–$A^*_{2\theta}$ orientations.

The $\{1\,1\,1\}$ pole figure for the initial sample is shown in Fig. 3a. The $\varphi_2 = 0^\circ$ and 45° sections of the ODF of the initial material are presented in Fig. 3b. A diagram showing the ideal shear and ideal ECAP texture components is also presented in this figure. The initial sample shows a weak <1 0 0> texture as well as presence of A^*_1 and A^*_2 components along with $\overline{B}$ component. As the shear plane is coincident with the 45° plane of the die, the corresponding components for ECAP textures are obtained by expressing the ideal orientations of simple shear in the ED–ND–TD reference system. This operation implies a rotation of 45° around the TD (or Z)-axis. The simple shear nature of the deformation process should lead to a monoclinic symmetry of the textures with respect to the TD axis, but this symmetry is not necessarily valid because the strain mode is not exactly a simple shear in the die. Experimental and theoretical flow line analyses as well as finite-element simulations have been shown that the ECAP deformation deviates from simple shear [26,27]. Monoclinic symmetry can be valid with a certain approximation in route A textures; this symmetry is definitely lost when the sample is subjected to route C strain path.

The changes in texture are quite apparent after deformation through ECAP die. $\{1\,1\,1\}$ pole figures shows weakening of the texture components after one pass (Fig. 4a). This weakening continues till 4 passes but the texture does not change between 4 and 8 passes as the $\{1\,1\,1\}$ pole figures for 4 and 8 passes in Fig. 4b and c show, respectively. A detailed analysis has been carried out using the ODF representation. The advantage of ODF lies in the fact that in orientation space the ideal orientations appear separately, without overlapping. The $\varphi_2 = 0^\circ$ and 45° sections of the ODFs after different ECAP passes are presented in Fig. 5. There are shifts from the ideal positions (compare with Fig. 3b); mostly shifts in the φ_1 direction of the ODF space meaning a rotation around the TD axis. Although some misalignment occurs in the texture measurement, but they affect the rotations around ND axis rather than TD axis.

After 1 pass, there are evolutions in $A^*_{1\theta}$ and C_θ texture components at $\varphi_2 = 0^\circ$ and also in $\overline{B}$component at $\varphi_2 = 45^\circ$ sections

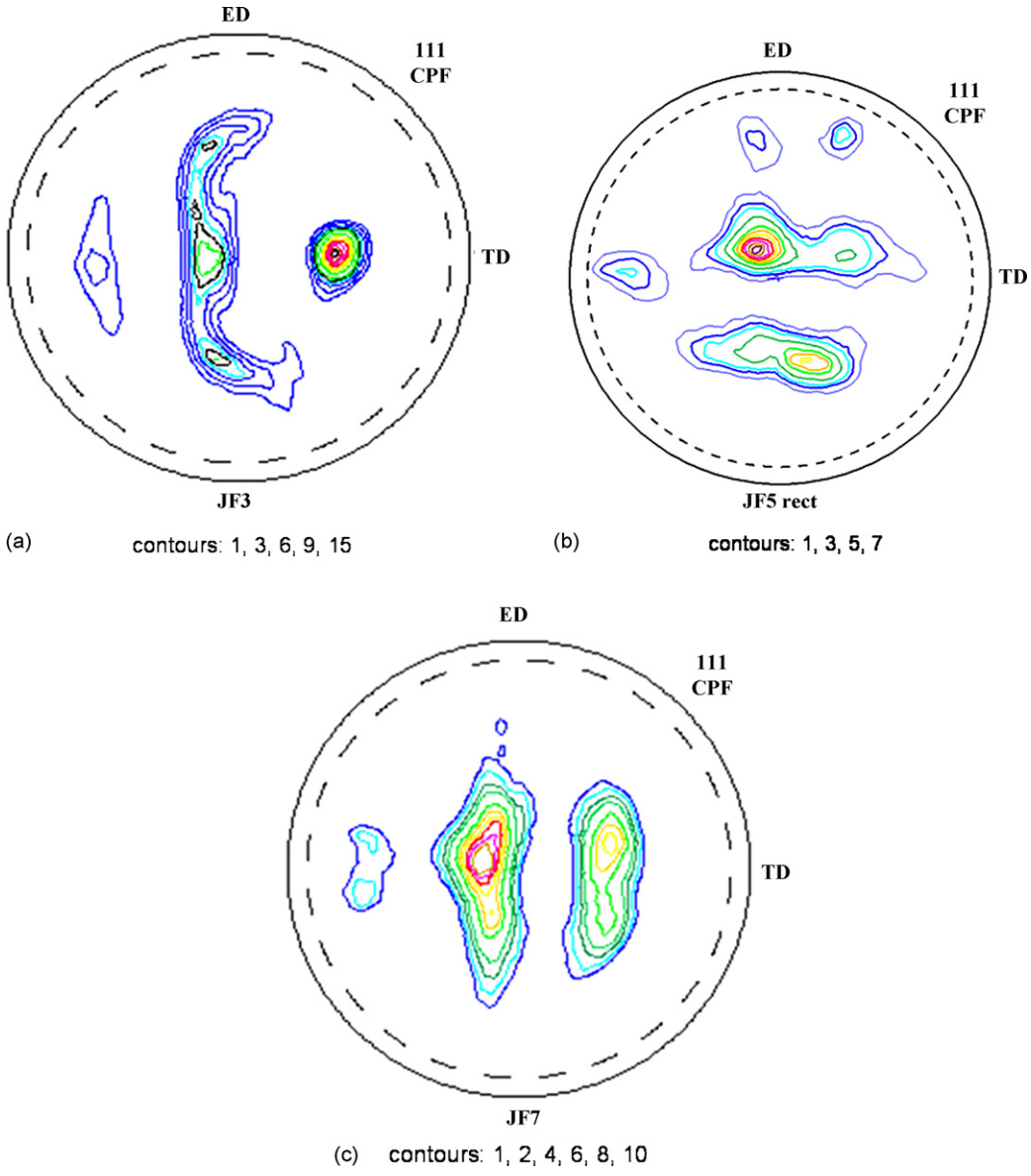

Fig. 4. {1 1 1} pole figures after (a) 1 pass, (b) 4 passes and (c) 8 passes.

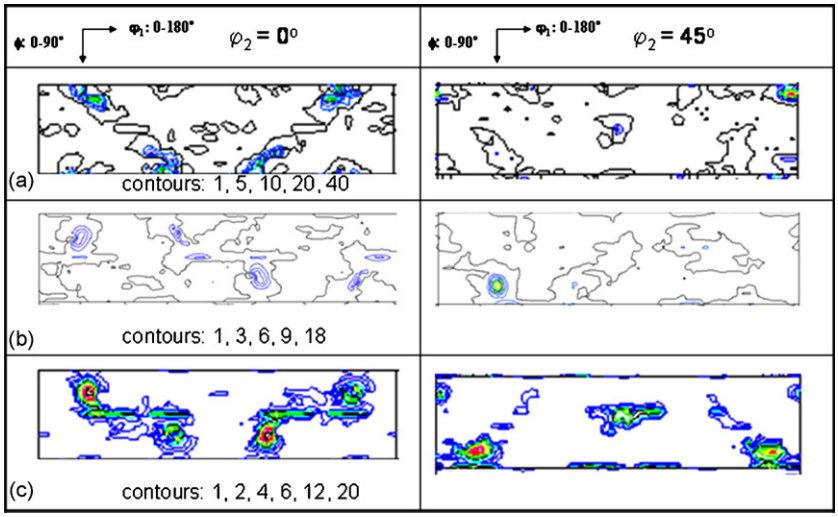

Fig. 5. ODF sections at $\varphi_2 = 0^\circ$ and 45° for (a) 1 pass, (b) 4 passes and (c) 8 passes.

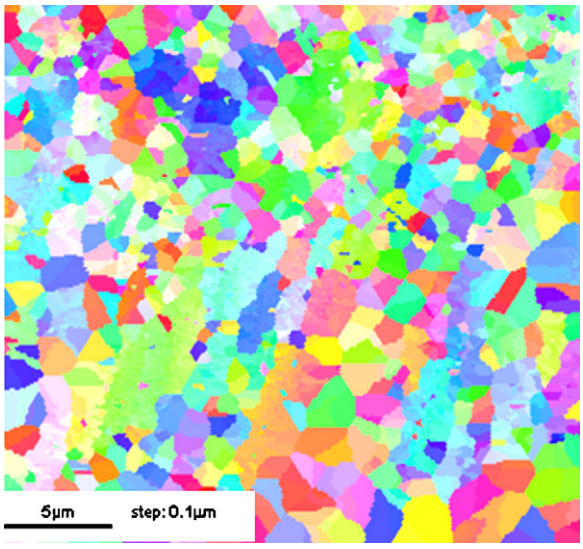

Fig. 6. Orientation map of sample processed by 8 passes.

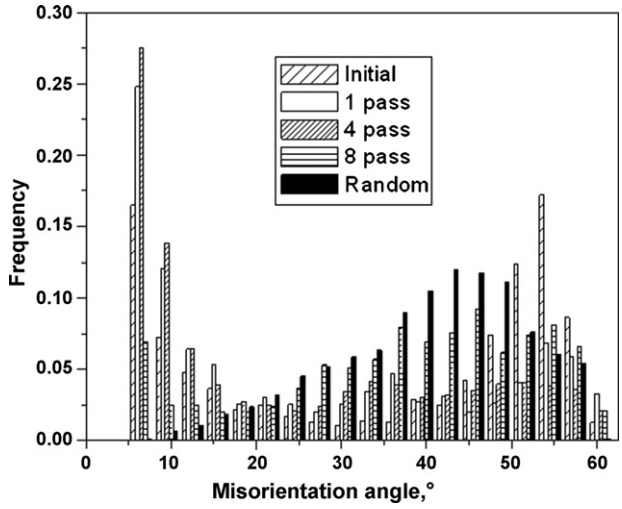

Fig. 7. Evolution of grain misorientation distribution with increasing number of ECAP passes.

(Fig. 5a). All of these components are shifted toward lower φ_1 values. Fig. 5b shows the evolution of similar components; however, these are deviated towards lower φ_1 values. After 4 passes the overall intensity of the texture is decreasing to half of that for 1 pass. After 8 passes, the texture components at $\varphi_2 = 0^\circ$ section is the same as after 4 passes but $\overline{A}$ component appears to replace $\overline{B}$ component observed up to 4 passes (Fig. 5c). The intensity of the texture is continuously decreasing with increasing number of passes; however, there were only slight changes in the textural components.

3.3. Evolution of grain boundary misorientation distribution

According to EBSD experiments, the grain size of the initial microstructure is observed to be ~20 μm. After 1 pass, the grain size reduces to ~4 μm. After 4 passes, the grain size is nearly 1 μm and there is only slight change in the grain size between 4 and 8 passes. The EBSD image after 8 passes is presented in Fig. 6. The misorientation distribution for different number of passes is plotted in Fig. 7. This figure shows that after 1 and 4 passes, there are mainly low angle grain boundaries. After 8 passes, the profile changes drastically. The average misorientation is ~37° after 8 passes which is close to the value corresponding to random orientation distribution (~42°).

4. Discussion

The crystallite size measured by X-ray line profile analysis and the grain size determined by EBSD saturate after 1 and 4 passes, respectively. Furthermore, the crystallite size measured by X-ray line profile analysis is one order of magnitude smaller than that measured by EBSD. This apparent discrepancy can be explained by the hierarchy of microstructure of ECAP-processed metals. In SPD-processed metals, the grains confined by high angle grain boundaries are subdivided into subgrains and/or cells [28]. In the evaluation of EBSD experiments, a grain is defined as the volume having boundaries with misorientations greater than 15°. At the same time the misorientation angles between neighbouring subgrains and cells are much smaller, usually only several degrees. The crystallites are defined as the domains in the material which scatter X-rays coherently. As the coherency of X-rays breaks even if they are scattered from volumes having quite small misorientations (1–2°), the crystallite size measured by X-ray line profile analysis corresponds rather to the subgrain size in the UFG microstructure. It should be noted that there are some specific dislocation configurations (e.g. dipolar dislocation walls) which also cause the disappearance of coherency of X-rays without any misorientation between the separated subgrains or cells [29]. The simultaneous application of X-ray line profile analysis and EBSD results in a detailed characterization of the hierarchical microstructure of SPD-processed materials.

Although the crystallite size (subgrain size) and the dislocation density saturated after 1 pass, the dislocation arrangement parameter, M, further decreased even up to 4 passes which indicates a stronger dipole character of the dislocation structure. In SPD-processed metals and alloys with medium or high stacking fault energy, the majority of dislocations can be found in the grain boundaries or subgrain boundaries [30]. Consequently, the decrease of the value of M indicates the evolution of boundary structure from a non-equilibrium state to a more equilibrated structure with less lattice distortions near the boundaries. This evolution is accompanied by the increase of boundary misorientations as it is suggested by the decrease of the grain size determined by EBSD. All the experiments in this study showed that there are no changes in the parameters of the microstructure (grain size, dislocation density) between 4 and 8 passes. At the same time, the grain orientation distribution changes even between 4 and 8 passes. The present EBSD experiments showed that in the initial state the fraction of high angle grain boundaries was small. During the first few passes a large amount of LAGBs develops by the arrangement of dislocations into dense structures. With increasing the number of ECAP passes, the average

misorientation increased and after 8 passes the fraction of high angle boundaries are quite high and the average misorientations is close to that of the randomly orientated grain structure.

Our experiments showed a weakening of the initial texture during ECAP processing. This can be explained by fragmentation of grain structure into subgrains which develop into grains with increasing strain. The highest scattering of the grain orientation was observed after 8 passes although there was no evolution of new texture components. The lack of new components may be explained by the fact that in route *C* the shear plane in the workpiece does not change between subsequent passes.

The present results of texture measurements are not consistent with the observations obtained previously on other ECAP-processed Al-based alloys. In the case of Al5056 alloy, there is a monotonous increase in the overall texture intensity with increasing number of passes [7]. For Al2024 alloy, the strength of the texture also increases with progressing deformation up to 8 ECAP passes [15]. At the same time, in the case of Al7034 alloy there is an initial weakening of the texture and subsequent strengthening during ECAP [16]. Moreover, after 1 ECAP pass, the texture evolution in Al7034 alloy deviates both from the ideal shear texture components and from the ideal ECAP texture components. This deviation is attributed to the strain relaxations associated with extensive precipitate fragmentation in the initial pass. After 6 passes of ECAP, the precipitate fragmentation in Al7034 alloy becomes essentially negligible and there is evidence for a gradual evolution towards the ideal ECAP texture. In our case the volume fraction of precipitates is relatively small and their fragmentation was not observed during ECAP which may explain the monotonous weakening of texture with increasing number of passes.

The yield strength determined by tensile test is listed in Table 1. The yield strength increases monotonously up to 8 passes even after the saturation of the parameters of the microstructure at 4 passes. This means that beside these parameters other microstructural features should affect the strength of ECAP-processed Al6082 alloy. This feature may be the structure of grain boundaries. Hernández Olivares and Gil Sevillano [31] showed that the more clustered the dislocation structure in the boundaries, the higher the strengthening effect of the boundaries. This means that the development of thinner, more equilibrated boundaries after 8 passes may increase the yield strength even in the lack of increasing the dislocation density or decreasing the grain size. It should be noted that the yield strength is also affected by the interaction between dislocations and Mg_2Si and $Mg_{12}Si_7Al_5$ precipitates.

It should be noted here that ECAP procedure may affect the precipitation structure. An example of this effect was demonstrated for a spray-cast Al7034 alloy which was subjected to ECAP at a temperature 473 K [32,33]. It has been shown that in this alloy the large rod-like $MgZn_2$ precipitates were broken by the high stresses imposed in ECAP to give a uniform distribution of very small spherical precipitates in the as-pressed material. The fragmentation of the rod-like precipitates resulted in a decrease of the flow stress. At the same time, the small, uniformly distributed precipitates stabilized the UFG structure even at high temperatures resulting in the improvement of superplastic behavior compared with the initial state before ECAP. For our Al6082 alloy the width of X-ray peaks of Mg_2Si and $Mg_{12}Si_7Al_5$ precipitates did not change significantly due to ECAP indicating that these precipitates did not fragmented into smaller parts during severe plastic deformation. Consequently, in our case the precipitates do not have significant contribution to the change of yield strength during ECAP.

5. Conclusions

The development of the dislocation density, the grain and subgrain sizes as well as the texture in Al6082 alloy processed by ECAP were investigated. The dislocation density and the subgrain size reached their maximum and minimum values, respectively, even after 1 pass. While the subgrain size did not change further, the grain size having high angle boundaries decreased up to 4 passes indicating the increase of the fraction of high angle grain boundaries between 1 and 4 passes. The grain orientation distribution reached the random case only after 8 passes which indicates that the grain boundary structure developed at least up to 8 passes. This observation is consistent with the diminishing of the initial texture during ECAP processing. The yield strength increased monotonously even after the saturation of the dislocation density and the grain size indicating that the more equilibrated high angle grain boundaries have higher strengthening effect than the non-equilibrium boundary structures.

Acknowledgements

This work was supported by the Hungarian Scientific Research Fund, OTKA, Grant No. F47057 and K67692 (JG). In addition, JG is grateful for the support of a Bolyai János Research Scholarship of the Hungarian Academy of Sciences. SGC, AM wishes to thank Prof. S.P. Mehrotra for his encouragement and kind permission to publish the paper.

References

[1] F. Dalla Torre, R. Lapovok, J. Sandlin, P.F. Thompson, C.H.J. Davies, E.V. Pereloma, Acta Mater. 52 (2004) 4819.
[2] R.Z. Valiev, T.G. Langdon, Prog. Mater. Sci. 51 (2006) 881.
[3] J.Y. Huang, X.Z. Liao, Y.T. Zhu, F. Zhou, E.J. Lavernia, Philos. Mag. 83 (2003) 1407.
[4] J.Y. Huang, Y.T. Zhu, H. Jiang, T.C. Lowe, Acta Mater. 49 (2001) 1497.
[5] X.Z. Liao, J.Y. Huang, Y.T. Zhu, F. Zhou, E.J. Lavernia, Philos. Mag. 83 (2003) 3065.
[6] R. Kaibyshev, K. Shipilova, F. Musin, Y. Motohashi, Mater. Sci. Eng. A 396 (2005) 341.
[7] C. Pithan, T. Hashimoto, M. Kawazoe, J. Nagahora, K. Higashi, Mater. Sci. Eng. A 280 (2000) 62.
[8] Q. Jining, Z. Di, Z. Guoding, J.-C. Lee, Scripta Mater. 51 (2004) 185.
[9] J.-H. Han, M.Y. Huh, J.-Y. Suh, J.-C. Lee, Mater. Sci. Eng. A 394 (2005) 60.
[10] Q. Jining, Z. Di, Z. Guoding, J.-C. Lee, Mater. Sci. Eng. A 408 (2005) 79.
[11] S. Akramov, M.G. Lee, I. Kim, D.Y. Sung, B.H. Park, Mater. Sci. Forum 475–479 (2005) 417.
[12] P.D. Wu, Y. Huang, D.J. Lloyd, Scripta Mater. 54 (2006) 2107.
[13] J.W. Signorelli, P.A. Turner, V. Sordi, M. Ferrante, E.A. Vieira, R.E. Bolmaro, Scripta Mater. 55 (2006) 1099.

[14] S.C. Baik, Y. Estrin, R.J. Hellmig, H.-T. Jeong, H.-G. Brokmeier, H.S. Kim, Z. Metallkd. 94 (2003) 1189.
[15] S.C. Wang, M.J. Starink, N. Gao, C. Xu, T.G. Langdon, Rev. Adv. Mater. Sci. 10 (2005) 249.
[16] S.G. Chowdhury, C. Xu, T.G. Langdon, Mater. Sci. Eng. A 473 (2008) 219.
[17] J. Gubicza, Gy. Krállics, I. Schiller, D. Malgin, Mater. Sci. Forum 473–474 (2004) 453.
[18] T. Ungar, J. Gubicza, G. Ribarik, A. Borbely, J. Appl. Crystallogr. 34 (2001) 298.
[19] G. Ribarik, T. Ungar, J. Gubicza, J. Appl. Crystallogr. 34 (2001) 669.
[20] E. Schafler, K. Simon, S. Bernstorff, P. Hanák, G. Tichy, T. Ungár, M.J. Zehetbauer, Acta Mater. 53 (2005) 315.
[21] P. Pawlik, Phys. Status Solidi (b) 134 (1986) 477.
[22] S. Li, I.J. Beyerlin, C.T. Necker, Acta Mater. 54 (2006) 1397.
[23] F. Montheillet, M. Cohen, J.J. Jonas, Acta Metall. 32 (1984) 2077.
[24] S. Li, I.J. Beyerlein, M.A.M. Bourke, Mater. Sci. Eng. A 394 (2005) 66.
[25] G.R. Canova, U.F. Kocks, J.J. Jonas, Acta Metall. 32 (1984) 211.
[26] M. Haouaoui, K.T. Hartwig, E.A. Payzant, Acta Mater. 53 (2005) 801.
[27] S.C. Baik, Y. Estrin, H.S. Kim, R.J. Hellming, Mater. Sci. Eng. A 351 (2003) 86.
[28] D.A. Hughes, N. Hansen, Acta Mater. 48 (2000) 2985.
[29] T. Ungár, G. Tichy, J. Gubicza, R.J. Hellmig, Powder Diffr. 20 (2005) 366.
[30] A. Mishra, B.K. Kad, F. Gregori, M.A. Meyers, Acta Mater. 55 (2007) 13.
[31] F. Hernández Olivares, J. Gil Sevillano, Acta Metall. 35 (1987) 631.
[32] C. Xu, M. Furukawa, Z. Horita, T.G. Langdon, Acta Mater. 51 (2003) 6139.
[33] C. Xu, M. Furukawa, Z. Horita, T.G. Langdon, Acta Mater. 53 (2005) 749.